SPECTRAL ANALYSIS ON REYNOLDS STRESS TRANSPORT EQUATION IN HIGH RE WALL-BOUNDED TURBULENCE

Myoungkyu Lee
Department of Mechanical Engineering
University of Texas at Austin
201 E 24th St, Austin, Texas 78712, USA
mk@ices.utexas.edu

Robert D. Moser
Department of Mechanical Engineerng
and Institute for Computational Engineering and Sciences
University of Texas at Austin
201 E 24th St, Austin, Texas 78712, USA
rmoser@ices.utexas.edu

ABSTRACT

Despite its importance in many applications, the nature of wall-bounded turbulent flow is not well-understood. The dynamics of near-wall turbulence has been well studied, with direct numerical simulation (DNS) making an important contribution. It has been difficult to study the interaction of near-wall and outer-layer turbulence via DNS because the Reynolds numbers available via DNS have not been sufficiently high to exhibit significant scale separation. In the work presented here, we correct that short-coming.

We have performed direct numerical simulation(DNS) of turbulent channel flow using a Fourier-Galerkin method in the streamwise(x) and spanwise (z) directions and a B-Splines collocation method in the wall-normal (y) direction. The highest Reynolds number based on shear velocity ($u_\tau = \sqrt{\tau_w/\rho}$), Re_τ is approximately 5200.

To study the scale dependence of the dynamics of the Reynolds stress components, we applied a spectral analysis to the terms in the Reynolds stress transport equation (RSTE). Result shows that the large (or very large) scale motion has an important role in turbulent transport terms. Also, it has been observed that a non-trivial portion of turbulent kinetic energy (TKE) is transported to the near-wall region and dissipated by large scale motion.

Introduction

Recently, much research has been directed at understanding wall-bounded turbulent flows at high Reynolds number (Re). Recent advances of experimental techniques (Nagib *et al.*, 2004; Kunkel & Marusic, 2006; Westerweel *et al.*, 2013; Bailey *et al.*, 2014) and computing power (Lee *et al.*, 2013; Borrell *et al.*, 2013; El Khoury *et al.*, 2013) provide information not previously available. One of the most important feature of high *Re* wall-bounded turbulence is the separation of scales between the near wall and outer layer turbulence. Two distinct peaks of the streamwise velocity energy spectral density are observed experimentally: a small-scale peak in the near-wall region and a large-scale peak in the outer region (Hutchins & Marusic, 2007; Monty *et al.*, 2009; Marusic *et al.*, 2010*a,b*). Two such spectral peaks were confirmed by direct numerical simulation(DNS) by Lee & Moser (2015). Lee & Moser (2015) have also found that there is peak distinction in the spectral density of Reynolds stress, $-u'v'$, but this has not yet been observed in experiments. Since the DNS can provides such richer data with high fidelity, it is possible to compute higher order terms in three dimensions. In this work, we have focused on the Reynolds stress transport equation (RSTE) which give us information about production, transport and dissipation of the Reynolds stress tenor. However, RSTE is an averaged equation, so it is difficult to study detailed roles of turbulent motions. Hence, we have performed a spectral analysis on each terms in RSTE to observe how the motions in different length scales contribute the transport of Reynolds stresses. To our knowledge, such a spectral analysis of terms in RSTE has not previously been performed. In this work we have focused on the turbulent kinetic energy (TKE) equation and the interaction between components of the velocity fluctuations.

This paper is organized as follow. First, the simulation methods and the definition of terms in RSTE are described. Then, the following are discussed: *Re* dependencies of terms in RSTE, spectral analysis of production, transport and dissipation, enhanced analysis of turbulent transport and interaction of velocity fluctuations in different direction by pressure-strain terms.

Table 1. Summary of simulation parameters. (Δx and Δz are in terms of Fourier modes for spectral methods. Δy_w and Δy_c are grid spacing at wall and center line, respectively. $Re_\tau = u_\tau \delta/\nu$, Tu_τ/δ - Total simulation time without transition)

Name	Re_τ	Re_b	Δx^+	Δz^+	Δy_w^+	Δy_c^+	Tu_τ/δ
R180	182	2,857	4.5	3.1	0.074	3.4	31.9
R550	544	10,000	8.9	5.0	0.019	4.5	13.6
R1000	1000	20,000	10.9	4.6	0.019	6.2	12.5
R2000	2003	43,478	12.3	6.1	0.323	8.9	11.
R5200	5186	125,000	12.7	6.4	0.498	10.3	7.80

Method

In the discussion to follow, the velocity components in streamwise(x), wall-normal(y), and spanwise(z) directions are denoted by u, v and w, respectively. Also, the mean velocities and fluctuations are denoted by capital letters and primes. Furthermore, $\langle \cdot \rangle$ denotes the expected value or average. Thus $U = \langle u \rangle$ and $u = U + u'$.

The incompressible turbulent flow between two infinite parallel planes is simulated. The lengths of simulation domain in x and z directions are truncated to $L_x = 8\pi\delta$ and $L_z = 3\pi\delta$ with periodic boundary conditions, where δ is the channel half width. No-slip and no-penetration boundary conditions at the walls are applied in y directions. A Fourier-Galerkin method is used in the x and z directions, while a seventh order B-spline collocation method is used in the y direction. The Navier-Stokes equations are manipulated to time-advance v and ω_y, the vorticity in the y direction (Kim *et al.*, 1987). Using this velocity-vorticity formulation is beneficial because continuity is exactly satisfied and the pressure term is eliminated. Time is discretized by a low-storage implicit-explicit method suggested by Spalart *et al.* (1991). The superscription, "+", indicates that the quantity is normalized by viscosity and friction velocity, $u_\tau = \sqrt{\tau_w/\rho}$, where τ_w denotes the mean shear stress at wall. The simulation parameters are provided in Table 1. More details about the simulation code, numerical methods, and simulation process are discussed in Lee *et al.* (2013, 2014); Lee & Moser (2015).

The equation for the velocity fluctuation is

$$\frac{\partial u_i'}{\partial t} = -U_k \frac{\partial u_i'}{\partial x_k} - u_k \frac{\partial U_i}{\partial x_k} - \frac{\partial u_k' u_i'}{\partial x_k} + \frac{\partial \langle u_k' u_i' \rangle}{\partial x_k} - \frac{\partial p'}{\partial x_i} + \nu \frac{\partial^2 u_i'}{\partial x_k \partial x_k}$$

Let $\tilde{u}_i' = u_i'(\tilde{\mathbf{x}})$, $\tilde{\mathbf{x}} = \mathbf{x} + \mathbf{r} = (x + r_x, y, z + r_z)$ where $\mathbf{r}$ is the separation vector in x and z direction. By multiplying the equation for $\partial u_i'/\partial t$ by $\tilde{u}_j'$, multiplying the equation for $\partial \tilde{u}_j'/\partial t$ by u_i', adding them and taking expected value, one obtains the following two-point correlation function which is a function of (r_x, y, r_z). Precisely:

$$\frac{\partial \langle u_i' \tilde{u}_j' \rangle}{\partial t} = P_{ij} + T_{ij} + \Pi_{s,ij} + \Pi_{d,ij} + D_{ij} - \varepsilon_{ij} \quad (1)$$

where

$$P_{ij} = -\langle \tilde{u}_j' v' \rangle \frac{\partial U_i}{\partial y} - \langle u_i' \tilde{v}' \rangle \frac{\partial U_j}{\partial y}$$

$$T_{ij} = \frac{\partial \langle \tilde{u}_j'(u'u_i') \rangle}{\partial r_x} - \frac{\partial \langle u_i'(\widetilde{u'u_j'}) \rangle}{\partial r_x} + \frac{\partial \langle \tilde{u}_j'(w'u_i') \rangle}{\partial r_z} - \frac{\partial \langle u_i'(\widetilde{w'u_j'}) \rangle}{\partial r_z}$$
$$- \frac{\partial \langle \tilde{u}_j'(v'u_i') \rangle}{\partial y} - \frac{\partial \langle u_i'(\widetilde{v'u_j'}) \rangle}{\partial y} + \left\langle (v'u_i') \frac{\partial \tilde{u}_j'}{\partial y} \right\rangle + \left\langle (\widetilde{v'u_j'}) \frac{\partial u_i'}{\partial y} \right\rangle$$

$$\Pi_{s,ij} = \left(\frac{\partial \langle p'\tilde{u}' \rangle}{\partial r_x} - \frac{\partial \langle \tilde{p}'u' \rangle}{\partial r_x} \right) \delta_{1i}\delta_{1j} + \left\langle p' \frac{\partial \tilde{v}'}{\partial y} + \tilde{p}' \frac{\partial v'}{\partial y} \right\rangle \delta_{2i}\delta_{2j}$$
$$+ \left(\frac{\partial \langle p'\tilde{w}' \rangle}{\partial r_z} - \frac{\partial \langle \tilde{p}'w' \rangle}{\partial r_z} \right) \delta_{3i}\delta_{3j} + \left\langle \tilde{p}' \frac{\partial u'}{\partial y} \right\rangle \delta_{1i}\delta_{2j}$$

$$\Pi_{d,ij} = -\left(\frac{\partial \langle p'\tilde{v}' \rangle}{\partial y} + \frac{\partial \langle \tilde{p}'v' \rangle}{\partial y} \right) \delta_{2i}\delta_{2j} + \left(\frac{\partial \langle p'\tilde{v}' \rangle}{\partial r_x} - \frac{\partial \langle \tilde{p}'u' \rangle}{\partial y} \right) \delta_{1i}\delta_{2j}$$

$$D_{ij} = \nu \frac{\partial^2 \langle u'\tilde{u}_j' \rangle}{\partial y \partial y}$$

$$\varepsilon_{ij} = 2\nu \left(\frac{\partial^2 \langle u'\tilde{u}_j' \rangle}{\partial r_x \partial r_x} + \left\langle \frac{\partial u_i'}{\partial y} \frac{\partial \tilde{u}_j'}{\partial y} \right\rangle + \frac{\partial^2 \langle u'\tilde{u}_j' \rangle}{\partial r_z \partial r_z} \right)$$

P, T, Π_s, Π_d, D and ε denote production, turbulent-transport, pressure-strain, pressure-transport, viscous transport and dissipation respectively. Note that the Reynolds stress transport equation is the special case of eq (1) when $r_x = r_z = 0$. Also, T_{ij} can be decomposed as following:

$$T_{ij} = T_{ij,0} + T_{ij,1} \quad (2)$$

where

$$T_{ij,0} = T_{ij} + \frac{1}{2} \left(\frac{\partial \langle \tilde{u}_j'(v'u_i') \rangle}{\partial y} + \frac{\partial \langle u_i'(\widetilde{v'u_j'}) \rangle}{\partial y} \right)$$

$$T_{ij,1} = -\frac{1}{2} \left(\frac{\partial \langle \tilde{u}_j'(v'u_i') \rangle}{\partial y} + \frac{\partial \langle u_i'(\widetilde{v'u_j'}) \rangle}{\partial y} \right)$$

In this form, $T_{ij,0} = 0$ when $r_x = r_z = 0$. The discrete Fourier transform is performed on each term of eq (1).

$$\mathscr{F}(r_x, y, r_z) = \sum_{k_x, k_z} \widehat{\mathscr{F}}(k_x, y, k_z) e^{ik_x r_x} e^{ik_z r_z}$$

where $\mathscr{F}$ is each term in eq (1), $\widehat{\mathscr{F}}$ is Fourier-transformed function of $\mathscr{F}$ and k_x and k_z are wavenumbers in streamwise and spanwise directions. The one-dimensional energy spectral density of $\mathscr{F}$ is defined as

$$E_{x,\mathscr{F}}(k_x, y) = \sum_{k_z} \left[\widehat{\mathscr{F}}(k_x, y, k_z) + \widehat{\mathscr{F}}(-k_x, y, k_z) \right]$$

$$E_{z,\mathscr{F}}(k_z, y) = \sum_{k_x} \left[\widehat{\mathscr{F}}(k_x, y, k_z) + \widehat{\mathscr{F}}(k_x, y, -k_z) \right]$$

Finally, in the results that follow we have pre-multiplied spectra and profiles by k_x, k_z and/or y when plotting on log scales to represent the contribution to the integral, since, for example,

$$\int_\Omega \mathscr{F} \, \mathrm{d}y = \int_{\Omega^*} y\mathscr{F} \, \mathrm{d}(\log y)$$

2
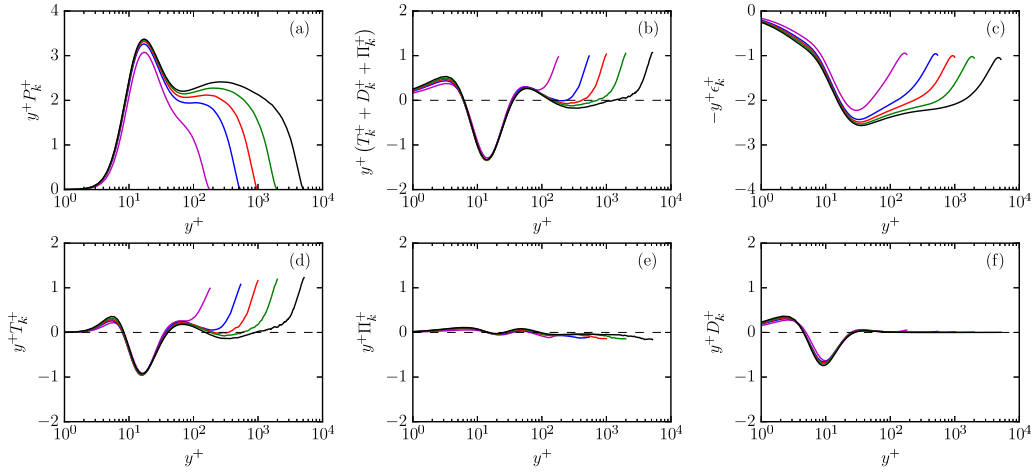
Figure 1. Production, transport and dissipation of turbulent kinetic energy: (a) Production (b) Transport (Turbulent+Pressure+Viscous) (c) Dissipation (d) Turbulent transport (e) Pressure transport (f) Viscous transport. R180: —— (Magenta), R550: —— (Blue), R1000: —— (Red), R2000: —— (Green), R5200: —— (Black)
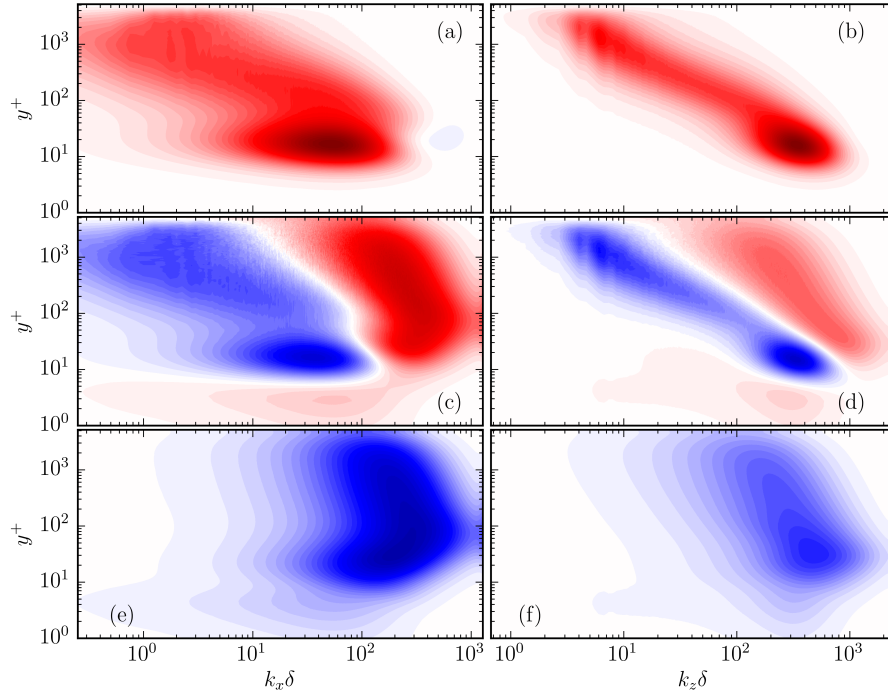
Figure 2. One-dimensional spectral density of production, transport and dissipation of turbulent kinetic energy for case R5200: (a) $y^+ k_x E_{x,P_k}$ (b) $y^+ k_z E_{z,P_k}$ (c) $y^+ k_x(E_{x,T_k} + E_{x,D_k} + E_{x,\Pi_k})$ (d) $y^+ k_z(E_{z,T_k} + E_{z,D_k} + E_{z,\Pi_k})$ (e) $-y^+ k_x E_{x,\varepsilon_k}$ (f) $-y^+ k_z E_{z,\varepsilon_k}$. Red is positive, white is zero and blue is negative.

Result

The one-dimensional profiles of terms in the Reynolds stress transport equation for turbulent kinetic energy, TKE ($k = \langle u_i' u_i' \rangle / 2$), are shown in figure 1. There are a few things that distinguish high Re flows from low Re flows. First, more TKE is produced and dissipated in the outer region as Reynolds number increases. Second, the transport of TKE becomes negative at $y^+ \approx 150$ in the flows with Re_τ greater than 1000 . This means that TKE is transported from the overlap region to inner or outer regions at high Re. Third, the dissipation appears to be developing a plateau as Re increases, though it may also be developing a sec-

ond peak. Also, the peak of the production increases with Reynolds number, though very slowly. The individual contributions to the transport term are shown in figure 1(d)-(f). It is clear that the turbulent transport is the most important mechanism at high Re, and the only term that shows strong Re dependencies. Note that the pressure strain term is analytically zero due to continuity, so figure figure 1(e) only reflects pressure transport. The data are available at http://turbulence.ices.utexas.edu.

The spectral density of the Reynolds stress transport equation for TKE in R5200 is shown in figure 2. All quantities are pre-multiplied by wall-normal distance and

3
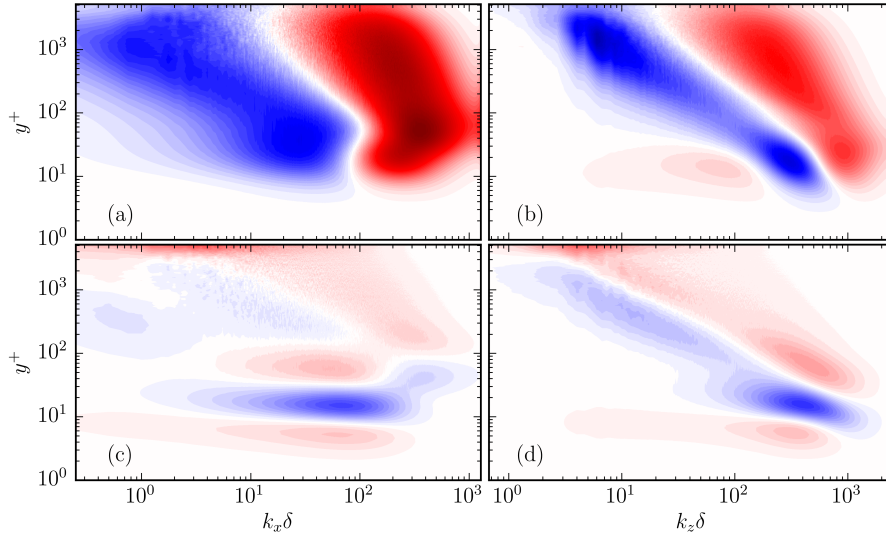
Figure 3. One-dimensional spectral density of turbulent transport of turbulent kinetic energy for case R5200: (a) $y^+ k_x E_{x,T_{k,0}}$ (b) $y^+ k_z E_{z,T_{k,0}}$ (c) $y^+ k_x E_{x,T_{k,1}}$ (d) $y^+ k_z E_{z,T_{k,1}}$. Red is positive, white is zero and blue is negative.
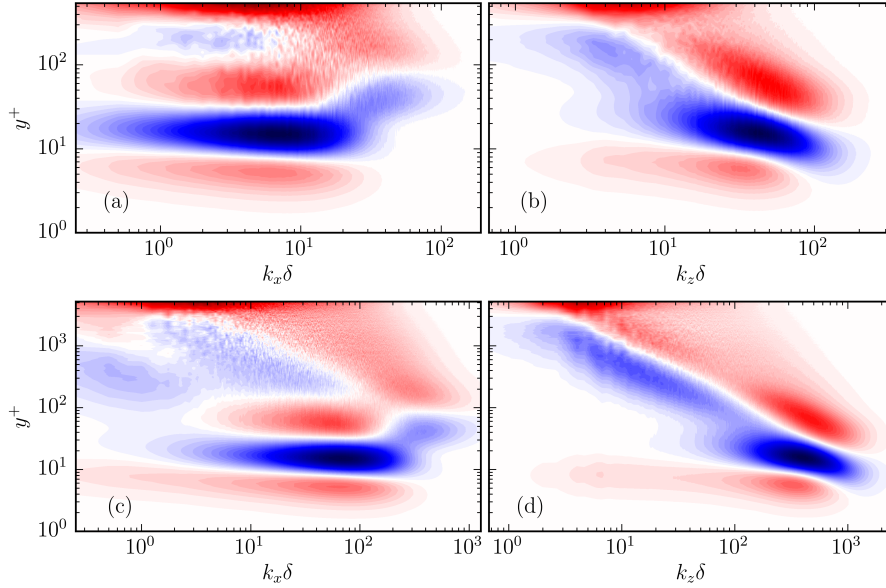
Figure 4. One-dimensional spectral density of transport of turbulent kinetic energy, $T_{k,1}$ (see eq (2)), for case R550(Top) and R5200(Bottom): (a) $y^+ k_x E_{x,T_{k,1}}$(R550) (b) $y^+ k_z E_{z,T_{k,1}}$(R550) (c) $y^+ k_x E_{x,T_{k,1}}$(R5200) (d) $y^+ k_z E_{z,T_{k,1}}$(R5200). Red is positive, white is zero and blue is negative.

wavenumber. In this flow, there are distinct inner- and outer- peaks in the spectra of $u'u'$ and $-u'v'$ from the flow at $Re_\tau \approx 5200$ (Lee *et al.*, 2013). Though it is hard to see in figure 2(a-b), there are also outer-peaks in pre-multiplied production at $k_x\delta \approx 2$ or $k_z\delta \approx 6$ and $y^+ \approx 1000$. This is expected because the production of TKE is the product of turbulent stress, $-\langle u'v'\rangle$, and the mean velocity gradient, $\langle \partial U^+/\partial y^+\rangle$. It is generally expected that the production of TKE will be positive. However, there is a small region where the spectral density of the production term is negative near $y^+ \approx 20$ and $k_x\delta \approx 600$. Such a negative region is not observed in the spanwise spectrum. The negative region is observed at approximately same wall-distance

and wavenumber at all Reynolds numbers simulated. Since $\langle \partial U^+/\partial y^+\rangle$ is always positive, the negative region of TKE production is from a negative region of the energy spectral density of $-u'v'$.

The spectral density of transport, which is the sum of turbulent, pressure and viscous transport terms is shown in figure 2(c-d). Three regions can be identified in the figure. First is the near-wall region (say $y^+ < 10$). TKE is transported into this region across a wide range of length scales, including very large scales with $k_x\delta < 1$. This transport at large scale presumably represents modulation of the near-wall flow by large-scale motions in the outer flow. The second region is $10 < y^+ < 100$. This region is distin-

4
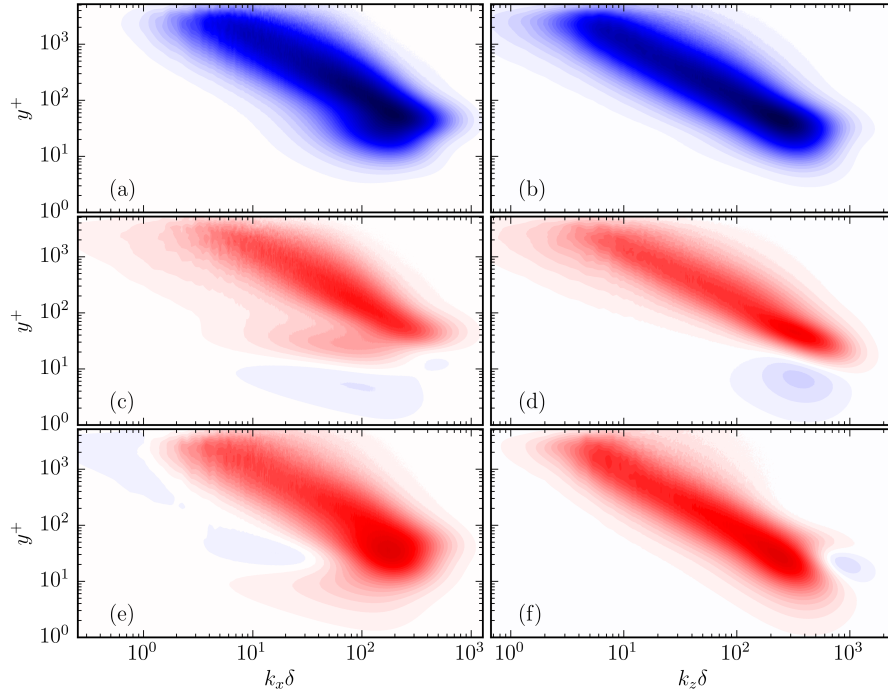
Figure 5. One-dimensional spectral density of pressure strain of velocity fluctuations: (a) $y^+ k_x E_{x,\Pi_{s,uu}}$ (b) $y^+ k_z E_{z,\Pi_{s,uu}}$ (c) $y^+ k_x E_{x,\Pi_{s,vv}}$ (d) $y^+ k_z E_{z,\Pi_{s,vv}}$ (e) $y^+ k_x E_{x,\Pi_{s,ww}}$ (f) $y^+ k_z E_{z,\Pi_{s,ww}}$, R5200 Red is positive, white is zero and blue is negative.

guished by negative peaks at around $y^+ \approx 20$, $k_x\delta \approx 30$ and $k_z\delta \approx 300$, with positive regions at higher wavenumbers. Note that $k_z\delta \approx 300$ implies a wavelength of approximate 100 plus units, consistent with the streak spacing. In the $y^+ > 100$ region, the negative and positive contribution to the transport shift to larger scale with increasing y^+. The negative part has an outer peak at $y^+ \approx 1000$. Also note that the variation in scale with y^+ of the negative contribution is more rapid than the positive part, especially in the x direction. The dissipation spectra follows the trend of the positive part of the transport spectra.

The turbulent transport is dominant among the transport terms as shown in figure 1. In figure 3, we have decomposed the turbulent transport as in (2). Figure 3(a-b) can be interpreted as TKE transfer in scale in the x and z directions, since for any y^+, the integral in k_x or k_z of these terms is zero. Figure 3(c-d) then represents TKE transport in the y direction. From these it is clear that for $y^+ > 100$, the transport term spectra shown in figure 2 are dominated by transfer of energy in scale in x and z. The more complicated structure is shown in the intermediate range, $10 < y^+ < 100$. Significant TKE transport across $y^+ \approx 100$ occurs at very small scales (say $k_x\delta \approx 400$). Large scales become more important to y-transport in the region, $y^+ > 100$, with a negative peak at $k_x\delta \approx 0.6$, in the very large scale motion (VLSM) regime. We compare $E_{T_{k,1}}$ form R5200 to $E_{T_{k,1}}$ in R550 in figure 4 to investigate the Reynolds number dependence. It was shown above that the turbulent transport terms goes negative as Reynolds number increases in the region, $y^+ > 150$ (Figure 1(b,d)). As shown in figure 4(a-b), the large scale negative contributions for $y^+ > 150$ are weak in R550. However, when Reynolds number increases, a clear VLSM structure is observed which acts as the key mechanism to transport TKE from outer to inner regions.

TKE is an important quantity characterizing the strength of turbulence, but results so far, have not allow us to see the interactions between the velocity components. Here, we have focus on pressure-strain term in the RTSE. Pressure-strain is the term that accounts for transfer of energy from $u'u'$ to $v'v'$ and $w'w'$. The spectral density of the pressure-strain terms are shown in figure 5. Note that the sum of spectral density of each components is zero at any wall-distance or wavenumber, i.e. $\sum_{k_x} (E_{x,\Pi_{s,uu}} + E_{x,\Pi_{s,vv}} + E_{x,\Pi_{s,ww}}) = 0$. As expected, $u'u'$ is not receiving energy from other components. The energy transfer between $v'v'$ and $w'w'$ is somewhat interesting. As shown in figure 5(c-d) the energy transfers from $v'v'$ to $w'w'$ near the wall. This can be explained by vertically moving fluids hitting the wall, the so-called "splat effect". It is observed that the energy of large scale motion of $w'w'$ is transported to $v'v'$ only in streamwise the direction. Also, the energy from very small scale motion of $w'w'$ at $k_z \approx 1000$ and $y^+ \approx 10$ transfers to other components only in the spanwise direction. The mechanism of this energy transfer is not clear.

5

Conclusion

The Reynolds stress transport equations are a great statistical tool to characterize the wall-normal dynamics of turbulence. But of course, transfer in scale is a critical turbulence phenomenon. Starting from the two-point correlation evolution equation, we performed spectral analysis to allow the study of scale dependence in RSTE. We observed that there is modulation of the near-wall flow by large (or very large) scale motion in outer region. Also, it is revealed that the large scale motions are important to the physics at overlap region, roughly at $100 < y^+ < 1000$, especially at high Reynolds number. The spectral analysis of pressure-strain terms similarly enabled study of the energy transfer between turbulent fluctuation in different directions. Surprisingly, energy transports from $w'w'$ to $v'v'$ by large scale motion in streamwise direction and small scale motion in spanwise direction were observed.

Investigation of the physical mechanisms responsible for the observations made here is ongoing. But, it is clear that the spectral analysis of the Reynolds stress transport equations is a powerful tool to analyze wall-bounded turbulence. A more detailed analysis of the turbulent transport term in overlap region is needed since it is the key quantity that displays differences between low and high Reynolds number flows. In addition to the velocity variance terms, the same analysis can be done for Reynolds shear stress, $-u'v'$.

REFERENCES

Bailey, S. C. C., Vallikivi, M., Hultmark, M. & Smits, A. J. 2014 Estimating the value of von Kármán's constant in turbulent pipe flow. *Journal of Fluid Mechanics* **749**, 79–98.

Borrell, Guillem, Sillero, Juan A. & Jiménez, Javier 2013 A code for direct numerical simulation of turbulent boundary layers at high Reynolds numbers in BG/P supercomputers. *Computers & Fluids* **80**, 37–43.

El Khoury, George K., Schlatter, Philipp, Noorani, Azad, Fischer, Paul F., Brethouwer, Geert & Johansson, Arne V. 2013 Direct Numerical Simulation of Turbulent Pipe Flow at Moderately High Reynolds Numbers. *Flow, Turbulence and Combustion* **91** (3), 475–495.

Hutchins, Nicholas & Marusic, Ivan 2007 Large-scale influences in near-wall turbulence. *Philosophical transactions. Series A, Mathematical, physical, and engineering sciences* **365** (1852), 647–664.

Kim, John, Moin, Parviz & Moser, Robert 1987 Turbulence statistics in fully developed channel flow at low Reynolds number. *Journal of Fluid Mechanics* **177**, 133–166.

Kunkel, Gary J. & Marusic, Ivan 2006 Study of the near-wall-turbulent region of the high-Reynolds-number boundary layer using an atmospheric flow. *Journal of Fluid Mechanics* **548**, 375–402.

Lee, Myoungkyu, Malaya, Nicholas & Moser, Robert D. 2013 Petascale direct numerical simulation of turbulent channel flow on up to 786K cores. In *Proceedings of SC13: International Conference for High Performance Computing, Networking, Storage and Analysis*. New York, New York, USA: ACM Press.

Lee, Myoungkyu & Moser, R. D. 2015 Direct numerical simulation of turbulent channel flow up to $Re_\tau \approx$ 5200. *Journal of Fluid Mechanics(submitted), arXiv* **1410.7809**.

Lee, Myoungkyu, Ulerich, Rhys, Malaya, Nicholas & Moser, Robert D. 2014 Experiences from Leadership Computing in Simulations of Turbulent Fluid Flows. *Computing in Science and Engineering* **16** (5), 24–31.

Marusic, Ivan, Mathis, Romain & Hutchins, Nicholas 2010*a* High Reynolds number effects in wall turbulence. *International Journal of Heat and Fluid Flow* **31** (3), 418–428.

Marusic, I., McKeon, B. J., Monkewitz, P. A., Nagib, H. M., Smits, A. J. & Sreenivasan, K. R. 2010*b* Wall-bounded turbulent flows at high Reynolds numbers: Recent advances and key issues. *Physics of Fluids* **22** (6), 065103.

Monty, J. P., Hutchins, N., Ng, H. C. H., Marusic, I. & Chong, M. S. 2009 A comparison of turbulent pipe, channel and boundary layer flows. *Journal of Fluid Mechanics* **632**, 431–442.

Nagib, Hassan, Christophorou, Chris, Reudi, Jean-Daniel, Monkewitz, Peter, Österlun, Jens & Gravante, Steve 2004 Can we ever rely on results from wall-bounded turbulent flows without direct measurements of wall shear stress. In *24th AIAA Aerodynamic Measurement Technology and Ground Testing Conference*, p. 2392. Portland, Oregon.

Spalart, Philippe R., Moser, Robert D. & Rogers, Michael M. 1991 Spectral methods for the Navier-Stokes equations with one infinite and two periodic directions. *Journal of Computational Physics* **96** (2), 297–324.

Westerweel, Jerry, Elsinga, Gerrit E. & Adrian, Ronald J. 2013 Particle Image Velocimetry for Complex and Turbulent Flows. *Annual Review of Fluid Mechanics* **45** (1), 409–436.